Korean J. Chem. Eng., 39(9), 2499-2504 (2022)
DOI: 10.1007/s11814-022-1087-2

pISSN: 0256-1115
eISSN: 1975-7220

Effect of air gap interval on polyvinylidene fluoride hollow fiber membrane spinning for CO_2 and CH_4 gas separation

Sie Hao Ding*,, Pei Ching Oh*,**,†, and Asif Jamil*****

*Department of Chemical Engineering, Universiti Teknologi PETRONAS, 32610 Seri Iskandar, Perak, Malaysia
**CO_2 Research Centre (CO2RES), Institute of Contaminant Management, Universiti Teknologi PETRONAS, 32610 Seri Iskandar, Perak, Malaysia
***Department of Chemical, Polymer and Composite Materials Engineering, University of Engineering and Technology Lahore (New-Campus), Pakistan
(*Received 1 November 2021 • Revised 10 February 2022 • Accepted 20 February 2022*)

Abstract−Improper control of air gap interval during hollow fiber membranes (HFMs) spinning may lead to structural defects such as inner lumen deformations and macrovoids**.** In the current work, PVDF HFMs were prepared by manipulating air gap intervals at 5, 10, 15, 20, and 25 cm, using dry-wet spinning mechanism. The changes in its properties, including contact angle, mechanical strength, and most importantly the morphological structure that is usually crucial for gas separation performance have been determined. The morphology was evaluated using SEM, and the inner lumen defects of HFMs were reduced with the increment of air gap interval during the spinning process. Subsequently, the CO_2 gas permeance was observed to increase from 5 to 15 cm air gap distance and almost constant at 20 cm air gap interval, then increase tremendously beyond this point. Furthermore, CO_2/CH_4 ideal selectivity was observed to be improved and reached the highest end at PVDF-AG15 and dropped beyond this point. Therefore, varying air gap distance is considered as a practical approach for better gas separation. However, macrovoids will form if the air gap length is overlong. Thus, optimum air gap length during PVDF HFMs spinning is vital for morphology and gas separation performance.

Keywords: Air Gap Interval, Polyvinylidene Fluoride, Hollow Fiber Membrane, Gas Separation

INTRODUCTION

Over the years, CO_2 concentration in the environment has increased tremendously and subsequently caused global warming [1-4]. Besides, the CO_2 in natural gas usually reacts with water and produces acidic properties that can damage a pipeline or other equipment. Thus, CO_2 elimination from natural gas is important from the aspect of environment and its calorific content. In the current separation technologies, the membrane gas separation process is favored over conventional processes due to its low cost, small footprint, and eco-friendliness [4-9]. Generally, membranes appear in hollow fiber and flat sheet configuration. However, hollow fiber membranes (HFMs) are more favorable due to their greater surface area and packing density [10-12]. Hence, interest in HFMs spinning for gas separation has been growing over time.

Polyvinylidene fluoride (PVDF) has been widely used in polymeric membrane production since it displays promising mechanical properties, thermal stability, and excellent chemical resistance [13]. However, usage of HFMs in industrial is limited due to defects in the membranes [14]. Structural defects are usually crucial and undesirable to performance testing, especially in gas separation. Nevertheless, researchers have reported that the defects of HFMs had been reduced by manipulating the spinning parameter [15-17]. Among the spinning parameters, air-gap distance is an essential and crucial parameter for the development of HFMs. For instance, Shi et al. found that increasing the air gap from 0.5 to 20 cm could overcome the inner contour deformation of PVDF-HFP HFMs, starting at 10 cm air gap distance [16]. Subsequently, Bonyadi et al. manipulated the air gap interval from 0 to 20 cm and found that by raising the air gap interval, the inner contour of the HFMs was reduced [18]. Zhang et al. observed that ideal annular conformation cross-section of Polyacrylonitrile HFMs formed with the longer air gap interval. The optimum air gap distance was reported to be 6.1 mm, ranging from 2.5 to 10 mm [19]. Ahmad and Shafie found that irregular lumen was produced at an air gap of 5 cm and a minimum of 10 cm air gap distance was needed to produce PES/PVA HFMs with regular inner lumen [20].

On the contrary, air gap distance on HFMs spinning had been reported to affect the gas separation performance. Mubashir et al. reported that CO_2/CH_4 ideal selectivity of cellulose acetate (CA) HFMs improved from 0.9 to 4.5 and was reduced to 2.5 when air gap interval increased from 0 to 5 cm and 5 to 7.5 cm, respectively [21]. Pak et al. also found that CO_2/CH_4 ideal selectivity of CA HFMs increased from 0.9 to 43.8 and fell to 15.4 when air gap distance increased from 10 to 15 cm and 20 cm, respectively [22]. Hosseini et al. observed that when air gap interval was increased from 1 to 3 cm, the dual-layer HFMs CO_2/CH_4 ideal selectivity improved from 1.38 to 3.05, respectively [23].

†To whom correspondence should be addressed.
E-mail: peiching.oh@utp.edu.my

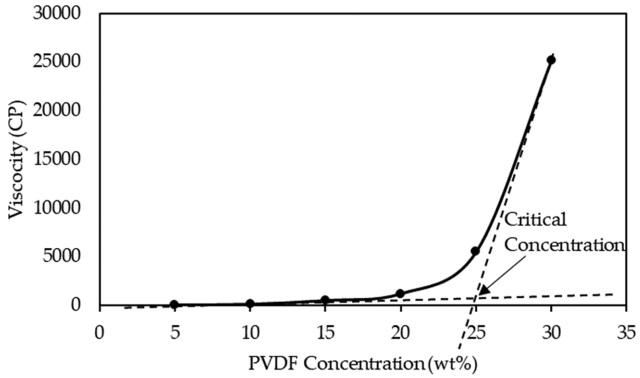

Fig. 1. Graph of PVDF concentration versus the viscosity of PVDF/NMP solutions.

Based on the above discussions, optimizing air gap distance during the hollow fiber spinning is essential and worth exploring. Although the great potential in reducing/eliminating defects in HFMs could be achieved by increasing air gap distance on HFMs spinning, yet minimal studies have been carried out on PVDF HFMs, and no report on its effect on CO_2/CH_4 gas separation. Therefore, this work's aim was to optimize the air gap distance on the PVDF hollow fiber spinning to study its morphology and properties on CO_2/CH_4 gas separation.

MATERIALS AND METHODS

1. Reagents and Materials

PVDF pellet (Mw ~180,000) was purchased from Sigma-Aldrich, and 1-Methyl-2-pyrrolidone (NMP, purity 99.5%) was purchased from Merck. All chemicals were used without purification.

2. Methods

2-1. Dope Solution Preparation

First, PVDF pellet was dried in the oven at 100 °C overnight. The critical concentration of PVDF/NMP solution was investigated using a protocol reported elsewhere [21]. Dope solutions with PVDF concentrations of 5, 10, 15, 20, 25, and 30 wt% were prepared. Next, a small amount of each resulting solution was transferred to a plastic tube for viscosity testing using a rotational viscometer at 50 rpm. Fig. 1 shows the graph of PVDF concentration versus the viscosity of PVDF/NMP solutions.

In Fig. 1, the critical concentration of PVDF/NMP was determined to be 25 wt%, where observed at the intersect of linear and tangent lines plotted over the viscosity curve [21]. Subsequently, 75 mL of 25 wt% PVDF/NMP dope solution was prepared and degassed for 30 minutes and then poured into a dope solution holder and left overnight prior to hollow fiber spinning.

2-2. Hollow Fiber Spinning

Fig. 2 shows the illustration of hollow fiber spinning machine utilized for the spinning of PVDF HFMs [21]. The current work adopted the dry-wet phase inversion mechanism for HFMs spinning as described elsewhere [21,24]. First, tap water was introduced as an internal bore fluid. Next, the bore fluid was supplied at 0.8 ml/min through the spinneret via the syringe pump. Subsequently, under nitrogen gas pressure (1 bar), the dope solution was pumped to the spinneret with a 1.8 ml/min rate. Finally, the spun fiber was allowed to pass through the external coagulant bath at ambient temperature. PVDF HFMs were spun with the air-gap distance ranging from 5 to 25 cm. The samples are denoted as PVDF-AG5, PVDF-AG10, PVDF-AG15, PVDF-AG20, and PVDF-AG25, respectively. Table 1 outlines the PVDF HFMs spinning parameters in the current work. All the spun HFMs were submerged in tap water for seven days to allow solvent elimination. PVDF HFMs

Table 1. Hollow fiber spinning conditions

Parameter	Condition
Dope solution	PVDF/NMP
PVDF concentration (wt%)	25
Air-gap distance (cm)	5-25
Bore fluid (tap water, wt%)	100
Bore flow rate (mL/min)	0.8
Spinneret dimensions (OD/ID, mm)	0.8/0.4
Dope flow rate (mL/min)	1.8
Coagulant temperature (tap water, °C)	Ambient temperature
Take-up speed (m/min)	Free fall

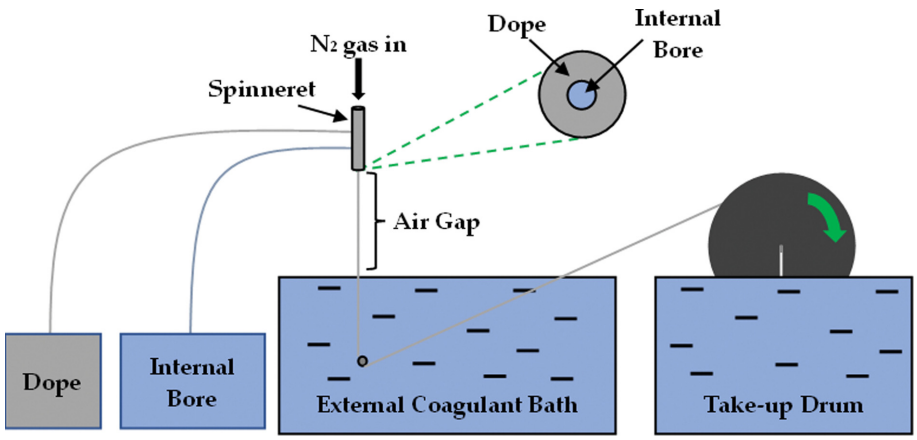

Fig. 2. Hollow Fiber spinning machine utilized for PVDF HFMs spinning.

were dried at ambient temperature before storage for future usage [21,25,26].

3. Characterization

3-1. Scanning Electron Microscopy (SEM)

SEM (Hitachi TM3030Plus) was utilized to reveal the cross-sectional structure of spun HFMs. The spun HFMs were cracked in liquid nitrogen. HFMs were stuck to the sample holder using carbon film and placed in the SEM. The images were viewed under an operating acceleration voltage of 15 kV at 150 k magnification.

3-2. Measurement of Contact Angle

The contact angle was measured by using a goniometer (Ramé-Hart Instrument Co.). A microsyringe was used to supply water on the external surface of HFMs to quantify its contact angle. Contact angles were measured three times on different spots, and then the mean value was determined.

3-3. Mechanical Properties Measurement

Mechanical analysis of HFMs involved using a tensile machine (Tinus Olsen H10KS-AP52276). Under the influence of applied stress, the tensile properties of HFMs were determined. The response of HFMs to the applied force was recorded in a stress-stress curve until it broke. To evaluate the stiffness of HFMs along with the maximum stress that the HFMs can tolerate, ultimate tensile strength (UTS), elastic modulus (E-Modulus), and percent elongation were evaluated. The test was done by using a load of 0.45 kN and a cross-head rate of 50 mm/min until the substrate fracture.

3-4. Gas Permeation Measurements

HFM module inserted with five fibers of effective length of 15 cm was attached with epoxy glue on one end to prevent gas pass through. In contrast, the other end of the pile remained open for the desired inlet gases. Next, the module was installed in the separation unit, and nitrogen gas was supplied to purge the system. Feed gas was then supplied to the system. At atmospheric pressure, the flow rate of permeate was taken using a bubble flowmeter after a stability duration of 30 minutes. Permeation flow rate was studied at feed pressure of 2 bar and room temperature. Fig. 3 illustrates the schematics of hollow fiber bundle preparation.

CO_2 permeance of HFMs was determined based on the following equation:

$$P_{CO_2}=Q/\Delta PA, \quad (1)$$

where Q is the CO_2 permeate flow rate of at standard pressure and temperature, ΔP is pressure different, and A is the effective area of the HFM. Permeance is given in gas permeation units (GPU), where 1 GPU is equal $1\ GPU=1\times10^{-6}\ cm^3(STP)/(cm^2\cdot s\cdot cm\cdot Hg)$. CH_4 permeance is calculated by using a similar procedure. CO_2/CH_4 ideal selectivity was calculated by dividing CO_2 and CH_4 permeance based on the following equation:

$$\alpha^*_{CO_2/CH_4}=P_{CO_2}/P_{CH_4} \quad (2)$$

RESULTS AND DISCUSSION

1. Morphological Analysis of PVDF HFMs

A cross-sectional morphology of PVDF HFMs spun at various air gap intervals ranging from 5 to 25 cm is shown in Fig. 4. Irregular inner lumen can be observed in Fig. 4(a) and (b). However, in (c), (d), and (e), with the continuous increase in air gap interval, the inner lumen deformation is reduced significantly. Since solvent diffusing out from a dope is consistently faster than bore fluid diffusing into the polymer dope, the shrinkage of pure PVDF HFMs during phase inversion is observed. This is because the lumen skin may be insufficiently rigid to suppress the inward radial force, which deforms the fiber's inner lumen [18,27]. In dry-wet spinning mechanism, the phase inversion between internal bore fluid and dope had already started before entering the external coagulant bath. There is adequate time for the hardening of the membrane to happen near the lumen of the PVDF HFMs, which consequently enables a more solidified lumen skin to form before the dope enters the external coagulant bath. Thus, PVDF HFMs with reduced inner lumen deformation can be spun when the air gap interval is high enough. Similar morphology has also been reported elsewhere [18, 20,27-30]. On the other hand, it can be seen that all the HFMs showed finger-like structures and macrovoids near the inner lumen, which is the most severe in Fig. 4(e). This is because when a larger air gap is applied, the internal bore fluid has longer contact time to intrude from the inner lumen of the membrane, causing the formation of larger voids [31-33].

2. Contact Angle Analysis

Table 2 shows the contact angle obtained for the spun PVDF HFMs. The contact angle of PVDF HFMs increased with increas-

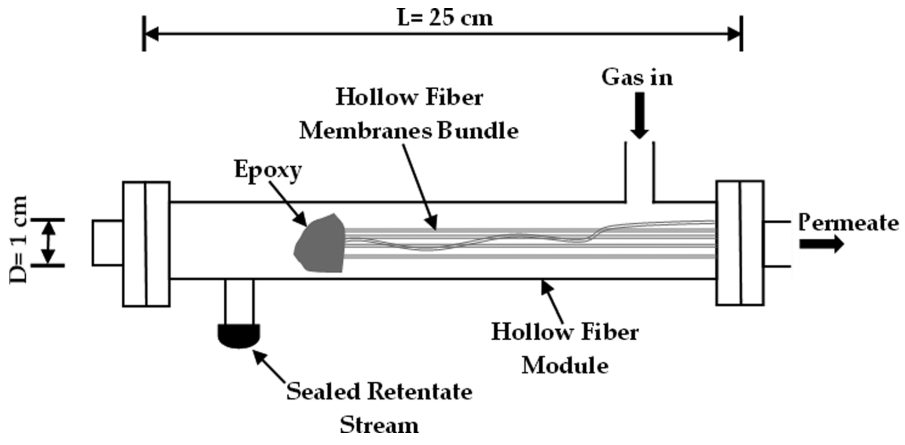

Fig. 3. Schematics of hollow fiber bundle preparation.

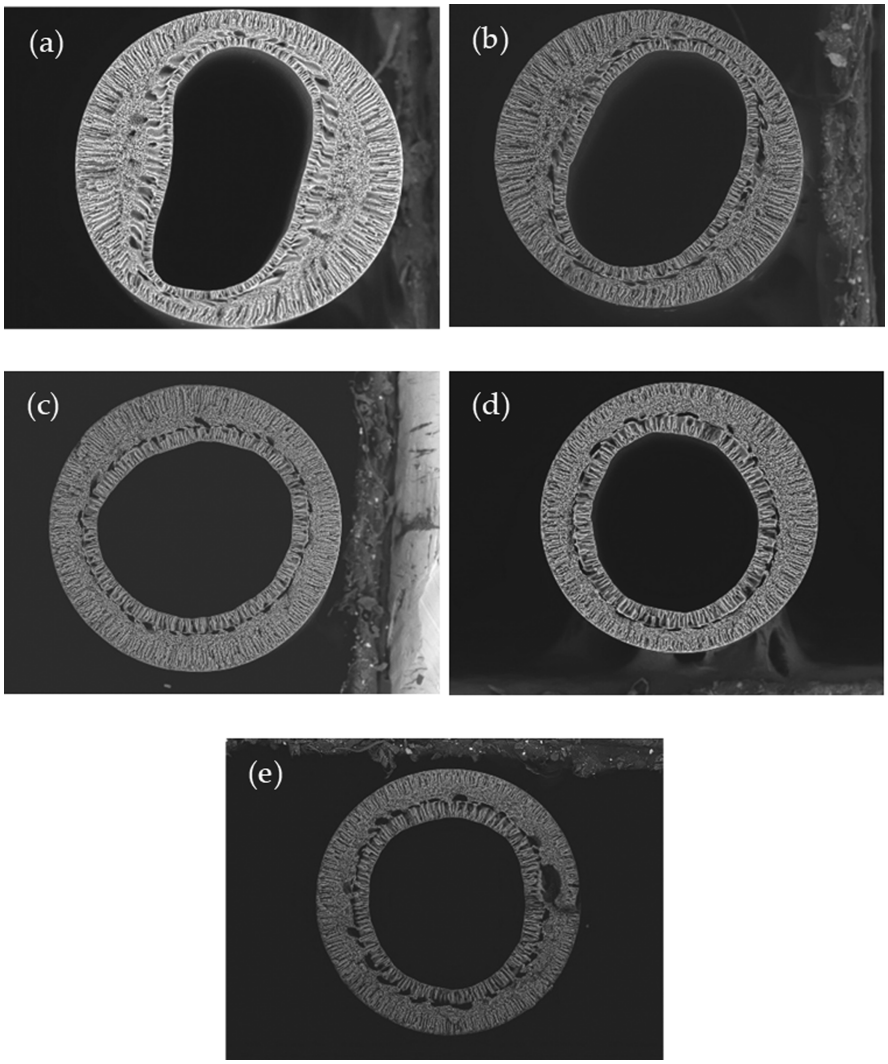

Fig. 4. Cross-sectional morphology of (a) PVDF-AG5, (b) PVDF-AG10, (c) PVDF-AG15, (d) PVDF-AG20, and (e) PVDF-AG25 at 150 k magnification.

Table 2. Contact angle of PVDF HFMs

Sample	Contact angle (°)
PVDF-AG5	86.65±0.43
PVDF-AG10	88.27±0.26
PVDF-AG15	95.16±6.63
PVDF-AG20	83.49±0.38
PVDF-AG25	82.09±4.87

ing air gap distances of 15 cm. Beyond this value, the contact angle subsequently decreased. This is because, more macrovoids formed especially in PVDF-AG25, as shown in Fig. 4. The increase in contact angle is due to a more compact and aligned membrane structure where water is more likely to be repelled by membrane's surface and less likely to diffuse into polymer matrix. It is also hypothesized that increasing the air gap on PVDF HFMs spinning would reduce the surface roughness, causing the membranes to exhibit increased hydrophobicity. Furthermore, macrovoids increased the porosity of membranes and caused the water droplet to possess higher tendency to diffuse into the matrix, causing reduced contact angle. Similar results have been reported elsewhere [34-37].

3. Mechanical Properties of PVDF HFMs

The effect of air gap interval (5 to 25 cm) on the mechanical properties of spun PVDF HFMs was analyzed and reported in tensile strength, E-modulus, and elongation at break. Table 3 shows the mechanical properties of spun PVDF HFMs. The tensile strength and elastic modulus increased when air gap distance increased from 5 to 15 cm but dropped when air gap interval was increased from 15 to 25 cm. From PVDF-AG5 to PVDF-AG15, and PVDF-AG15 to PVDF-AG25, it can be observed that the tensile strength increased around 8% and dropped about 12%, respectively. The tensile strength improvement with elevated air gap interval might be due to a more compact and oriented polymer chain during the spinning process, as shown in Fig. 4. Since more severe macrovoids formed beyond PVDF-AG15, the tensile strength of the spun HFMs was affected as macrovoids, reducing the mechanical strength of membranes. The trend of mechanical strength in this work is in

Table 3. Mechanical properties of spun PVDF HFMs

Sample	Tensile strength (MPa)	E-modulus (MPa)	Elongation at break (%)
PVDF-AG5	1.14	16.05	60.00
PVDF-AG10	1.17	18.61	79.60
PVDF-AG15	1.23	26.46	86.20
PVDF-AG20	1.20	26.24	83.50
PVDF-AG25	1.10	25.48	82.30

agreement with results reported elsewhere [30,38-40].

On the other hand, the E-modulus of spun PVDF HFMs also showed a similar trend. E-modulus is the measure of a membrane's resistance towards elastic deformation when stress is applied. An improvement of approximately 64% was achieved when air gap interval was increased from 5 to 15 cm, and reduced approximately 4% beyond 15 cm distance. Lastly, the elongation at break for PVDF-AG15 was highest, showing that it has the highest resistance to change without breaking. Thus, PVDF-AG15 has the optimum mechanical properties among the spun PVDF HFMs.

4. Effect of Air Gap Interval on Single Gas Permeation

Fig. 5 shows the graph of different air-gap distances influence on single gas permeation performance of PVDF HFMs. From Fig. 5, CO_2 permeance shows increment from PVDF-AG5 to PVDF-AG15, remains constant at PVDF-AG20, and further increases at PVDF-AG25. The CO_2 permeance shows improvement around 100% and 232% when air gap interval was raised from 5 to 20 cm and 20 to 25 cm, respectively. On the other hand, CH_4 permeance shows a linear increment up to 20 cm and further increases at 25 cm air gap distance. The CH_4 permeance improved around 82% and 430% when air gap distance was increased from 5 to 20 cm and 20 to 25 cm, respectively. The data analysis shows that the percentage improvement of CO_2 permeance is greater when compared to the improvement of CH_4 permeance up to 20 cm air gap distance. Nevertheless, the percentage improvement trend leveled off at PVDF-AG25. The improvement in CO_2 and CH_4 gas permeance could be due to the improvement of PVDF HFMs inner lumen morphology, which usually favors gas permeation. The sudden gas permeance increment beyond 20 cm air gap interval would probably due to the severe macrovoids formed in the HFMs, as discussed in Fig. 4. The discussion on SEM images also supports the CO_2/CH_4 ideal selectivity trend, which shows improvement by around 23% when air gap distance increases from 5 to 15 cm and starts to decline around 43% at 25 cm compared to PVDF-AG15. The improvement is due to a more uniform molecular orientation when air gap distance increases. However, above the maximum tolerance of air-gap distance, polymer chain packing may weaken and produce finger-like macrovoids, which is detrimental for gas separation performance. Similar results were reported by Mubashir et al. when CA HFMs spun by overlong air gap distance, weakened membrane chain packing and macrovoids were investigated [21]. PVDF-AG15 spun at optimum condition showed the highest CO_2/CH_4 ideal selectivity of 2.92±0.20, which was slightly lower than the reported results by Maity et al. who fabricated flat sheet PVDF membrane by dry-wet phase inversion method [41]. Despite this, another work by Kamble et al. obtained CO_2/CH_4 ideal selectivity less than 1 for the asymmetric PVDF flat-sheet membrane [42]. The comparison shows the ideal selectivity of spun PVDF in the current study is within an acceptable range. Moreover, the trend of CO_2/CH_4 ideal selectivity in this study strongly agrees with results reported elsewhere [21-23].

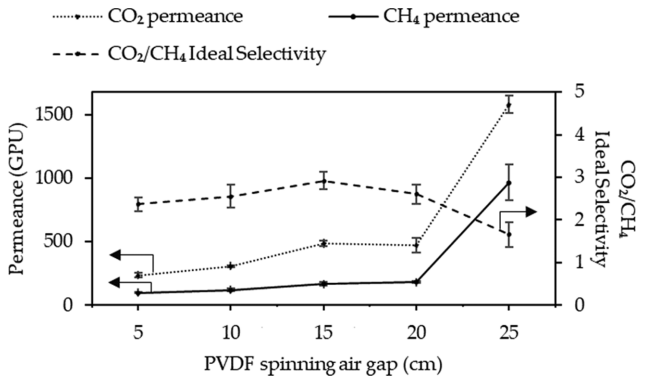

Fig. 5. CO_2 and CH_4 permeance, and CO_2/CH_4 ideal selectivity of PVDF-AG5, PVDF-AG10, PVDF-AG15, PVDF-AG20, and PVDF-AG25.

CONCLUSIONS

The effect of air gap distance on PVDF HFMs for CO_2/CH_4 separations has been reported. Cross-sectional morphology verified that the increase in air gap length would reduce the inner lumen defects. However, when over its maximum tolerance, more and larger macrovoids were produced, which subsequently increased the porosity of membranes.

PVDF-AG15 showed the highest contact angle at 95.16±6.63, and mechanical analysis suggested that PVDF-AG15 had the most mechanical strength among the spun PVDF HFMs. These results are probably due to the more packed and aligned polymer chain orientation formed and macrovoids formed along with the increment of air gap length during HFMs spinning, which agrees with the SEM images.

The gas permeation results obtained showed that CO_2 permeance improved with increasing air gap interval from 5 to 25 cm, except for constant value between PVDF-AG15 and PVDF-AG20. Meanwhile, CO_2/CH_4 ideal selectivity showed optimum for PVDF-AG15 with the value of 2.92±0.20. The current results are mostly attributed to the effect of air gap length on PVDF HFMs spinning, where it improves the polymer orientation/morphology and consequently improves the CO_2/CH_4 gas separation performance. Therefore, optimizing air gap length on PVDF HFMs spinning was very effective for improving its physical properties and morphology to obtain better CO_2/CH_4 gas separation performance. The optimum HFM spun in this work was determined to be PVDF-AG15.

ACKNOWLEDGEMENTS

We would like to express our gratitude for the financial support received from Ministry of Higher Education, Malaysia, FRGS

(Ref. No. FRGS/1/2018/TK02/UTP/02/3, Cost Center 015MA0-003) and YUTP-Fundamental Research Grant (Cost Centre: 015LC0-105). In addition, the technical support provided by the CO_2 Research Centre (CO2RES), Institute of Contaminant Management, is duly acknowledged.

AUTHOR CONTRIBUTIONS

Conceptualization, S.H.D. and P.C.O.; Methodology, S.H.D. and P.C.O.; Investigation, S.H.D.; Analysis, S.H.D. and P.C.O.; Supervision, P.C.O., and A.J.; writing—original draft, S.H.D.; writing – review and editing, S.H.D. and P.C.O.

FUNDING

This research was funded by the Ministry of Higher Education, Malaysia, under Fundamental Research Grant Scheme (FRGS) (Ref. No. FRGS/1/2018/TK02/UTP/02/3, Cost Center 015MA0-003) and YUTP-Fundamental Research Grant (Cost Centre: 015LC0-105).

CONFLICT OF INTEREST

The authors declare no conflict of interest. The funders had no role in the design of the study; in the collection, analyses, or interpretation of data; in the writing of the manuscript, or in the decision to publish the results.

REFERENCES

1. A. Awad and I. H. Aljundi, *Korean J. Chem. Eng.*, **35**, 1700 (2018).
2. M. Mubashir, Y. F. Yeong, T. L. Chew and K. K. Lau, *Sep. Purif. Technol.*, **215**, 32 (2019).
3. L. Ma, F. Svec, T. Tan and Y. Lv, *ACS Appl. Nano Mater.*, **1**, 2808 (2018).
4. L. Meng, X. Zou, S. Guo, H. Ma, Y. Zhao and G. Zhu, *ACS Appl. Mater. Interfaces*, **7**, 15561 (2015).
5. M. Mubashir, Y. Y. Fong, C. T. Leng and L. K. Keong, *Chem. Eng. Technol.*, **41**, 235 (2018).
6. Z. Qiao, Q. Xu and J. Jiang, *J. Membr. Sci.*, **551**, 47 (2018).
7. A. Jamil, O. P. Ching, T. Iqbal, S. Rafiq, M. Zia-Ul-Haq, M. Z. Shahid, M. Mubashir, S. Manickam and P. L. Show, *J. Hazard. Mater.*, **41**, 126000 (2021).
8. S. Shahid, G. V. Baron, J. F. M. Denayer, J. A. Martens, L. H. Wee and I. F. J. Vankelecom, *J. Membr. Sci.*, **620**, 118943 (2021).
9. A. Shakoor, A. L. Khan, P. Akhter, M. Aslam, M. R. Bilad, I. M. Maafa, K. Moustakas, A. S. Nizami and M. Hussain,, *Environ. Sci. Pollut. Res.*, **28**, 12397 (2021).
10. X. Chen, *Asian Philos*, **27**, 1 (2017).
11. L. Hu, J. Cheng, Y. Li, J. Liu, J. Zhou and K. Cen, *J. Appl. Polym. Sci.*, **135**, 45765 (2018).
12. H. Pang, H. Gong, M. Du, Q. Shen and Z. Chen, *Sep. Purif. Technol.*, **191**, 38 (2018).
13. Y. Tang, Y. Lin, H. Lin, C. Li, B. Zhou and X. Wang, *Membranes (Basel)*, **10**, 1 (2020).
14. W. Li, *Prog. Mater. Sci.*, **100**, 21 (2019).
15. N. Peng, N. Widjojo, P. Sukitpaneenit, M. M. Teoh, G. G. Lipscomb, T.-S. Chung and J.-Y. Lai, *Prog. Polym. Sci.*, **37**, 1401 (2012).
16. L. Shi, R. Wang, Y. Cao, C. Feng, D. T. Liang and J. H. Tay, *J. Membr. Sci.*, **305**, 215 (2007).
17. W. Li, P. Su, G. Zhang, C. Shen and Q. Meng, *J. Membr. Sci.*, **495**, 384 (2015).
18. S. Bonyadi, T. S. Chung and W. B. Krantz, *J. Membr. Sci.*, **299**, 200 (2007).
19. X. Zhang, Y. Wen, Y. Yang and L. Liu, *J. Macromol. Sci. B*, **47**, 1039 (2008).
20. A. L. Ahmad and Z. M. H. Mohd Shafie, *J. Phys. Sci.*, **28**, 185 (2017).
21. M. Mubashir, Y. F. Yeong, K. K. Lau and T. L. Chew, *Polym. Test.*, **73**, 1 (2019).
22. S.-H. Pak, Y.-W. Jeon, M.-S. Shin and H. C. Koh, *Environ. Eng. Sci.*, **33**, 17 (2016).
23. S. S. Hosseini, N. Peng and T. S. Chung, *J. Membr. Sci.*, **349**, 156 (2010).
24. A. Huang and B. Feng, *J. Membr. Sci.*, **548**, 59 (2018).
25. Y.-w. You, C.-f. Xiao, Q.-l. Huang, Y. Huang, C. Wang and H.-l. Liu, *RSC Adv.*, **8**, 102 (2018).
26. H. Zhu, X. Jie, L. Wang, G. Kang, D. Liu and Y. Cao, *RSC Adv.*, **6**, 69124 (2016).
27. C. H. Loh and R. Wang, *J. Membr. Sci.*, **466**, 130 (2014).
28. M. Rahbari-Sisakht, A. F. Ismail, D. Rana and T. Matsuura, *J. Membr. Sci.*, **415**, 221 (2012).
29. Z. Wang and J. Ma, *Desalination*, **286**, 69 (2012).
30. F. Korminouri, M. Rahbari-Sisakht, D. Rana, T. Matsuura and A. F. Ismail, *Sep. Purif. Technol.*, **132**, 601 (2014).
31. E. Anuar, S. M. Saufi and H. W. Yussof, *Korean J. Chem. Eng.*, **36**, 1124 (2019).
32. F. Korminouri, M. Rahbari-Sisakht, T. Matsuura and A. F. Ismail, *Chem. Eng. J.*, **264**, 453 (2015).
33. S. M. Rosid, H. Hasbullah, Y. Raharjo, A. F. Ismail, M. H. D. Othman, S. H. S. A. Kadir, F. Kamal, M. S. Abdullah and B. C. Ng, *Mater. Today: Proc.*, **46**, 1929 (2021).
34. Y.-H. Zhao, B.-K. Zhu, X.-T. Ma and Y.-Y. Xu, *J. Membr. Sci.*, **290**, 222 (2007).
35. F. L. Huang, Q. Q. Wang, Q. F. Wei, W. D. Gao, H. Y. Shou and S. D. Jiang, *Express. Polym. Lett.*, **4**, 551 (2010).
36. M. Chan and S. Ng, *AIP Conf. Proc.*, **2016**, 20035 (2018).
37. H. S. Zakria, M. H. D. Othman, R. Kamaludin and A. Jilani, *IOP Conf. Ser.: Mater. Sci. Eng.*, **1142**, 12014 (2021).
38. H. A. Tsai, D. H. Huang, S. C. Fan, Y. C. Wang, C. L. Li, K.-R. Lee and J.-Y. Lai, *J. Membr. Sci.*, **198**, 245 (2002).
39. M. Khayet, *Chem. Eng. Sci.*, **58**, 3091 (2003).
40. M. R. M. Abed, S. C. Kumbharkar, A. M. Groth and K. Li, *J. Membr. Sci.*, **407**, 145 (2012).
41. B. Maity, R. K. R. A. L. Kanasan and S. Abdul Rahman, *Mater. Today: Proc.*, **41**, 136 (2021).
42. A. R. Kamble, C. M. Patel and Z. V. P. Murthy, *Sep. Sci. Technol.*, **54**, 311 (2018).